Structure and Malonyl CoA-ACP Transacylase Binding of *Streptomyces coelicolor* Fatty Acid Synthase Acyl Carrier Protein

Christopher J. Arthur[†], Christopher Williams[†], Katherine Pottage[§], Eliza Płoskoń[†], Stuart C. Findlow[§], Steven G. Burston[‡], Thomas J. Simpson[†], Matthew P. Crump[†,*], and John Crosby[†,*]

[†]School of Chemistry, University of Bristol, Cantock's Close, Bristol BS8 1TS, U.K., [‡]Department of Biochemistry, University of Bristol, School of Medical Sciences, University Walk, Bristol BS8 1TD, U.K., and [§]School of Biological Sciences, University of Southampton, Bassett Crescent East, Southampton SO16 7PX, U.K.

There have been a number of studies into the binding of acyl carrier proteins (ACPs) by fatty acid synthase (FAS) enzymes. In the first of these, the structure of *Bacillus subtilis* holo acyl carrier protein synthase (ACPS) in complex with ACP was solved by X-ray crystallography (*1*). Here a series of conserved acidic residues on helix II of ACP formed salt bridges to reciprocally charged lysine and arginine residues on the ACPS. Binding of *Escherichia coli* FAS ACP with FabH (*2*) and FabG (*3*) was similarly driven, which led to the hypothesis that residues along the length of helix II of ACP provide a commonly recognized interface. The FabI-ACP complex structure (*4*) suggests that the interface does not extend along the entire length of helix II of ACP but is limited to residues at the base of this helix. Thus, although the proteins that bind ACP may recognize ACP using many of the same contacts, the specific nature of those contacts may vary.

Dissociable type II FASs utilize the enzyme malonyl Coenzyme A-ACP transacylase (MCAT, FabD) for the formation of malonyl ACP (*5*). The structure of MCAT from the model actinomycete *Streptomyces coelicolor* (*Sc*) was solved in 2003, and a model for the complex with *Sc* actinorhodin (act) polyketide synthase (PKS) ACP was suggested (*6*). This model proposes a largely hydrophobic interaction, with the ACP orientated such that the loop region between helices I and II of ACP interacts with MCAT. In this orientation, the leucine of the conserved ACP DSL motif inserts into a hydrophobic pocket adjacent to the MCAT active site entrance while the aspartate of the same motif forms a salt bridge with a conserved lysine residue. This model is mechanistically

ABSTRACT Malonylation of an acyl carrier protein (ACP) by malonyl Coenzyme A-ACP transacylase (MCAT) is fundamental to bacterial fatty acid biosynthesis. Here, we report the structure of the *Steptomyces coelicolor* (*Sc*) fatty acid synthase (FAS) ACP and studies of its binding to MCAT. The carrier protein adopts an α-helical bundle structure common to other known carrier proteins. The *Sc* FAS ACP shows close structural homology with other fatty acid ACPs and less similarity with *Sc* actinorhodin (act) polyketide synthase (PKS) ACP where the orientation of helix I differs. NMR experiments were used to map the binding of ACP to MCAT. This data suggests that *Sc* FAS ACP interacts with MCAT through the negatively charged helix II of ACP, consistent with proposed models for ACP recognition by other FAS enzymes. Differential roles for residues at the interface are demonstrated using site-directed mutagenesis and *in vitro* assays. MCAT has been suggested, moreover, to participate in bacterial polyketide synthesis *in vivo*. We demonstrate that the affinity of the polyketide synthase ACP for MCAT is lower than that of the FAS ACP. Mutagenesis of homologous helix II residues on the polyketide synthase ACP suggests that the PKS ACP may bind to MCAT in a different manner than the FAS counterpart.

*Corresponding authors,
john.crosby@bristol.ac.uk,
matt.crump@bristol.ac.uk.

consistent in that it places the ACP in a position where it can access the active site of MCAT. More recently, a docking study of the interaction of *Helicobacter pylori* MCAT with its FAS ACP substrate has been reported (*7*). This suggested that ACP and MCAT interact through the negatively charged residues of helix II of ACP and positively charged residues around the MCAT active site.

To date, no biochemical evidence to support either of these MCAT-ACP models has been reported. It is important to note that while the *H. pylori* ACP-MCAT model uses the cognate FAS ACP, the *S. coelicolor* study used the *Sc* act PKS ACP structure, as the structure of the corresponding FAS ACP was unavailable. PKS and FAS ACPs are, however, generally not interchangeable, and thus their mode of interaction may be different. Furthermore, alternative mechanisms for PKS ACP malonylation exist that do not involve MCAT (*8*). We now report the structure of the *Sc* FAS ACP and studies that allow the nature of the interaction of the FAS and PKS ACPs with *S. coelicolor* MCAT to be differentiated.

RESULTS AND DISCUSSION

Structure of Sc FAS apo ACP. To act as the basis of our studies of ACP-MCAT binding, we first solved the structure of the *Sc* FAS apo ACP. Unambiguous assignments of spin systems were made using standard multidimensional multinuclear NMR experiments, and the Ambiguous Restraints for Iterative Assignment of NOEs (ARIA) protocol was used to automatically assign NOEs (*9*). One hundred structures were generated in the final calculation, based on 1811 NOEs, of which 443 were long-range (Table 1). Twenty structures were selected on the basis of their energetic favorability, lack of restraint violations, and small deviations from ideal bonds and angles (Figure 1, panel a). The model with the lowest root-mean-square distance (rmsd) to the average was selected as the representative structure (Figure 1, panel b). Experimental restraints were well satisfied with, on average, one NOE violation exceeding 0.3 Å (Table 1). Coordinates have been deposited in the protein databank under the code 2cnr.

Sc FAS ACP consists of four well-defined helices, helix I (Gln5 to Ile19), helix II (Ser41 to Glu52), helix III (Asp61 to Asn66), and helix IV (Arg70 to Met79) linked by three principal loop regions (Figure 1, panel d). The longest loop connects helices I and II and runs from Ala20 to Asp40. Residues 29–37 comprise a well-structured turn followed by a short stretch of residues

TABLE 1. Structural statistics and quality indicators for the most representative structure and the ensemble of 20 Sc FAS ACP structures

NOE restraints	Unambiguous	Ambiguous
Intraresidue NOEs	769	38
Sequential NOEs	362	53
Medium range NOEs	237	54
Long range NOEs	443	213

Dihedral angle restraints		
Backbone Ψ and Φ	120	
Hydrogen bond restraints	39	
rmsd to mean for backbone atoms	0.34 ± 0.06	
rmsd to mean for heavy atoms	1.29 ± 0.18	

Average no. of NOE violations		
>0.3 Å (per structure)		1
>0.5 Å (per structure)		0

	Representative structure	Ensemble
Ramachandran plot regions		
in most favored (%)	93.3	91.8
in additional allowed (%)	6.7	7.9
in generously allowed (%)	0.0	0.3
in disallowed (%)	0.0	0.0
rmsd from ideal geometry		
bonds (Å)	0.0040	0.0037 ± 0.0001
angles (deg)	0.58	0.57 ± 0.01
improper (deg)	1.7	1.8 ± 0.1

that connect to helix II. In contrast, loops 2 and 3 are significantly shorter. A number of ACPs have been reported to exist in more than one conformation, and it has been suggested that switching between these might serve as a control mechanism for ACP recognition (*10, 11*). In this case, however, we find no evidence for slow, two-state exchange in the *Sc* FAS apo ACP, with only a single set of cross peaks observed in the NMR spectra.

Comparison of the overall fold of *Sc* FAS ACP with FAS ACPs from *B. subtilis* (*12*) (PDB code 1hy8) and *E. coli* (*13*) (PDB code 1tk8) reveals, as expected, a con-
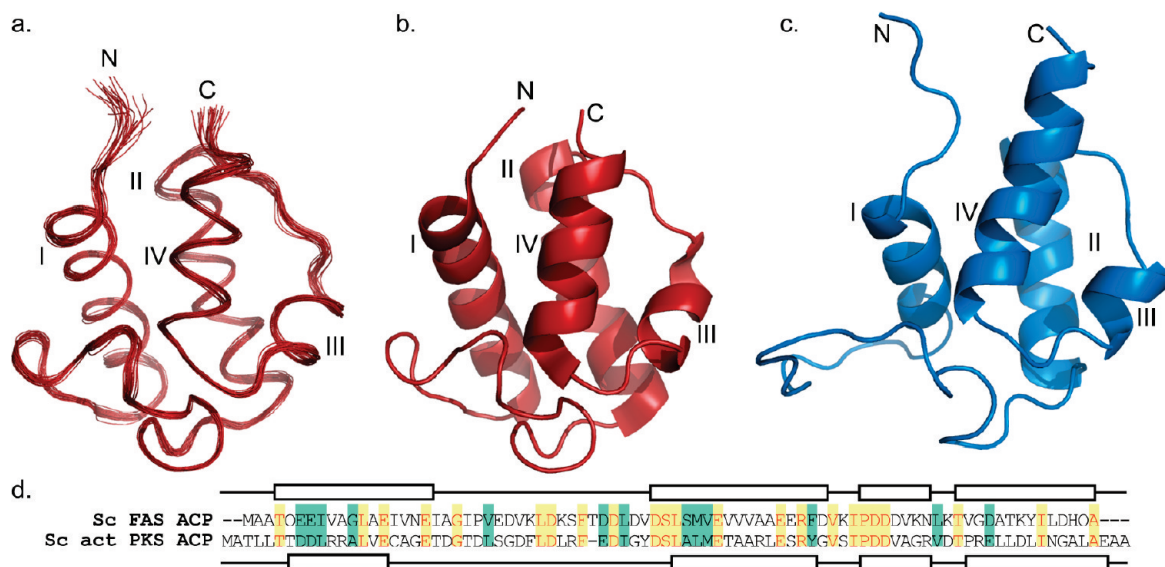
Figure 1. Structure of *Sc* FAS ACP and comparison to the *Sc* act PKS ACP (PDB code 2k0y) (*14, 15*). a) Ensemble of the 20 lowest energy structures. b) Representative structure of *Sc* FAS apo ACP. c) Average structure of *Sc* act PKS ACP. The α-carbons of both ACPs have been aligned with one another and are orientated with helices I and IV presented toward the reader. d) Sequence alignment of *Sc* FAS ACP and *Sc* act PKS ACP. Positions of helices are indicated. Amino acids on a yellow background are those that are identical in both ACPs, whereas those on a green background are residues that are chemically similar in both ACPs. All structures were drawn using PyMOL (*36*).

served relative orientation of the four helices (Figure 2, panel a). Superposition of backbone atoms for *Sc* FAS ACP residues 11−19;41−55;65−74 with *B. subtilis* (6−14;36−50;65−74) and *E. coli* (6−14;36−50;65−74) yields RMSDs of 1.52 and 1.85 Å (*E. coli vs B. subtilis* yields a fit of 1.41 Å). Despite a high degree of sequence similarity (28.7% identical, 42.5% similar, Figure 1, panel d) with its polyketide synthase counterpart, the *Sc* act PKS ACP (Figure 1, panel c, PDB code 2k0y) (*14, 15*), the structures of the two ACPs show differences in both helix I and loop 1. Superposition of residues from Sc act PKS ACP 42−74 (encompassing helices II, III, and IV) with residues 41−73 of *Sc* FAS ACP gives an rmsd of 1.58 Å, whereas superpositions including helix I gave poorer fits. Figure 2, panel b shows a superposition of the two structures showing the clear displacement of helix I in the PKS ACP. Loop 1 is also shorter and structurally better defined in the Sc FAS ACP with an rmsd over residues 18−28 of 0.21 ± 0.08 Å *vs* 1.93 Å in the Sc act PKS structure but bears a similar number of charged and polar residues along its length (Figure 1, panel d). The aspartate (Asp40) of the FAS ACP DSL motif is located at the base of helix II, whereas in the *Sc* act PKS

ACP the homologous residue is situated on the loop that precedes this helix.

Docking of FAS ACP with MCAT. The majority of biochemical and biophysical studies of ACP binding suggest that highly conserved residues on helix II of ACP interact electrostatically with reciprocally charged residues at the active site opening of its binding partner. Such a model for the binding of *H. pylori* MCAT with FAS ACP has been proposed (*7*). An alternate model for ACP recognition by MCAT has been suggested by Keatinge-Clay *et al.* (*6*), where MCAT recognizes a largely hydrophobic surface presented by the loop region between helix I and II of act PKS ACP (Figure 3, panel a). Unlike Keatinge-Clay *et al.*, who had only the *Sc* act PKS ACP structure available to them, we could utilize the *Sc* FAS ACP structure, the primary substrate for MCAT, and thus re-examine the *in silico* macromolecular docking of these proteins. Three algorithms were used in this analysis: ZDock (*16*), GRAMM-X (*17*), and ClusPro (*18*). Each of these has been assessed in the critical assessment of prediction of interactions blind protein docking experiment (*19*).

ZDock produced two distinct clusters of ACP−MCAT complex. The first closely mimics the model reported by
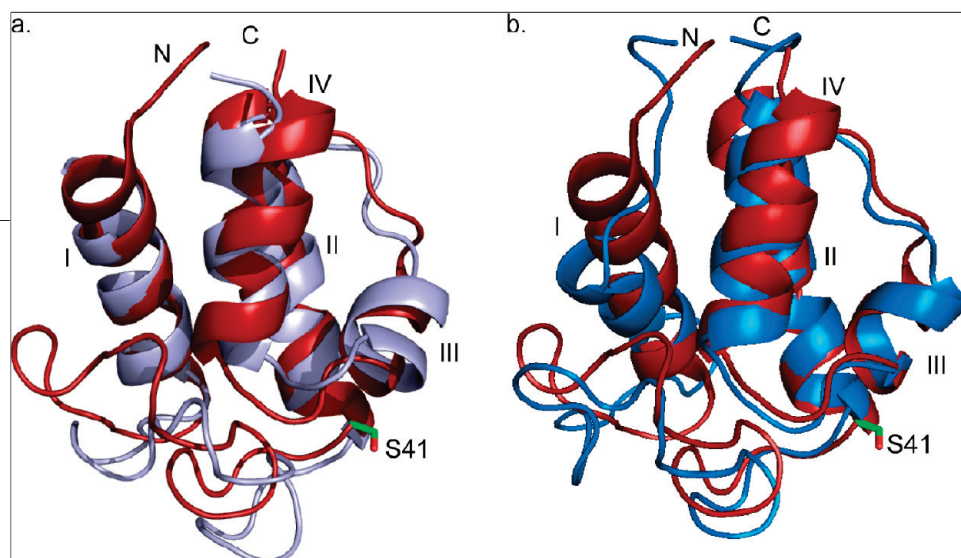
Figure 2. Structural superposition of FAS and PKS ACPs. a) Superposition of *Sc* FAS ACP over residues 6–14;36–50;65–74 (red) and *B. subtilis* ACP (*12*) residues 11–19;41–55;70–79 (mauve) oriented with helices I and II toward the reader. b) *Sc* FAS ACP superimposed over residues 41–73 with *Sc* act PKS ACP residues 42–74 (blue).

Keatinge-Clay *et al.* (*6*), with the *Sc* FAS ACP binding to residues surrounding the MCAT active site through the loop region between helix I and II (Figure 3, panel b). The second cluster packs helix II of *Sc* FAS ACP against MCAT (Figure 3, panel c), in a manner consistent with that suggested for *H. pylori* MCAT (*7*) and other ACP binding proteins. The ClusPro algorithm generated one cluster of carrier protein complexes in the proximity of the MCAT active site (Figure 3, panel d). Though similar,

these models are rotated with respect to both the Keatinge-Clay (Figure 3, panel a) and ZDock (Figure 3, panel b) complexes. Finally, the GRAMM-X algorithm returned only one complex where the ACP is adjacent to the MCAT active site. This model suggests that the ACP interacting surface is formed by helix IV (Figure 3, panel e). This is mechanistically unreasonable, however, as it orients the phosphopantetheine attachment site away from the MCAT active site.
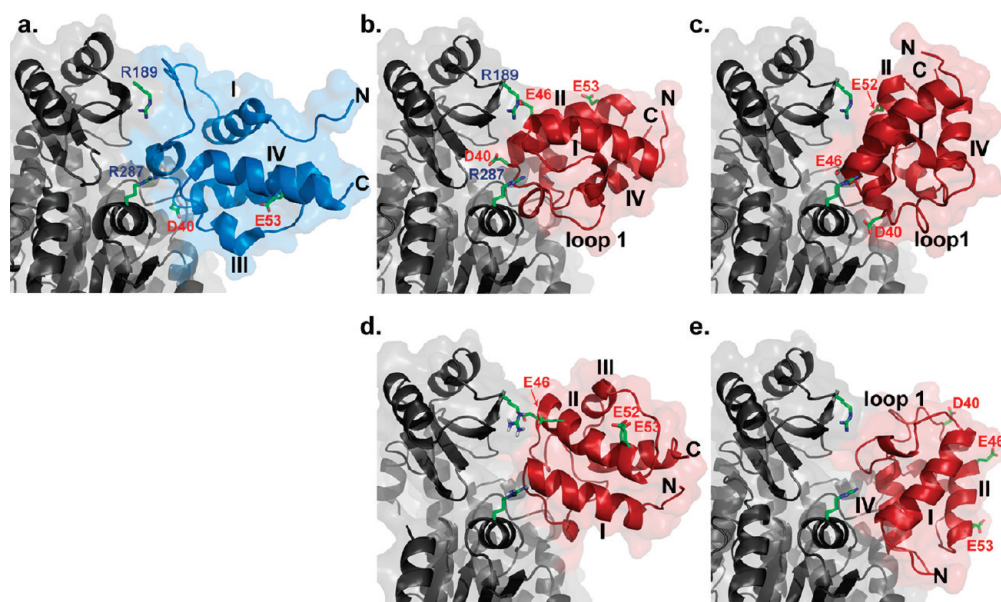
Figure 3. Docked ACP-MCAT models. MCAT (gray) has been aligned in each figure. Selected MCAT and ACP residues are represented as sticks to help orientate the reader. a) Keatinge-Clay model of *Sc* act PKS ACP (blue) with MCAT (PDB code 1nnz) (*6*). b) Representative of ZDock models that suggest binding through the loop region between helices I and II of *Sc* FAS ACP (red) and MCAT. c) Representative of ZDock models that suggest that *Sc* FAS ACP interacts with MCAT through helix II of ACP. d) Model obtained using ClusPro that suggests that *Sc* FAS ACP interacts through the loop region between helices I and II. e) Model determined using the GRAMM-X algorithm that suggests that *Sc* FAS ACP interacts *via* helix IV of ACP.
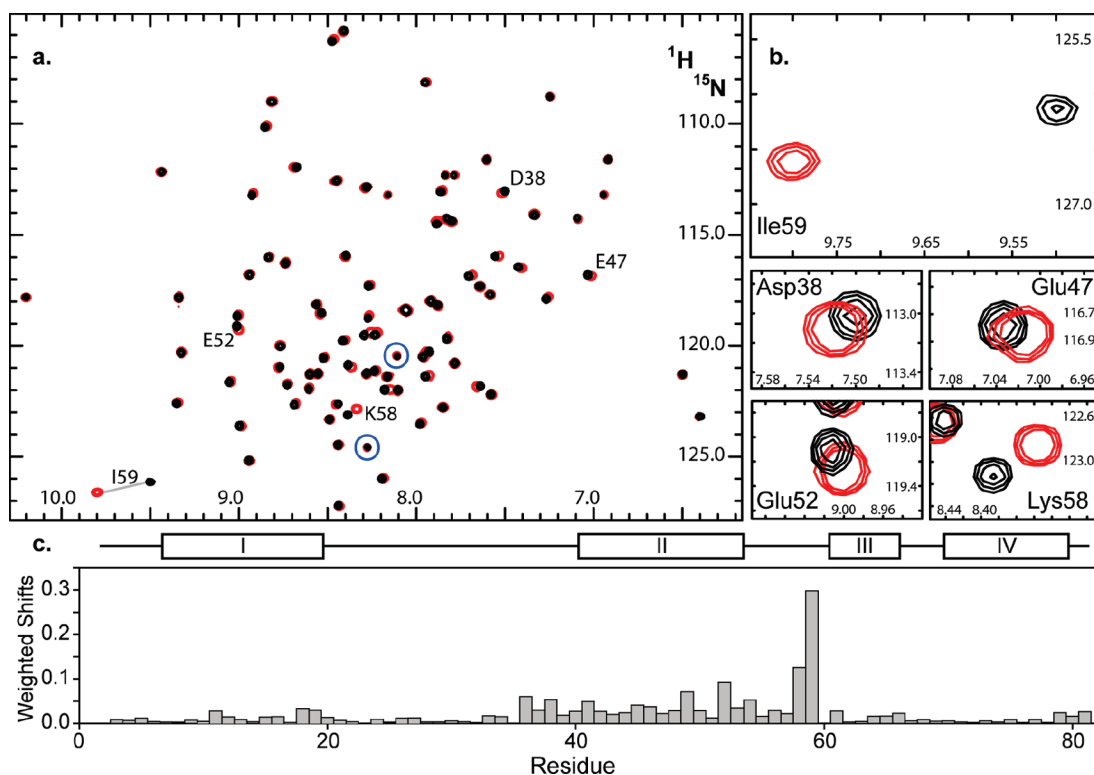
Figure 4. a) Superimposed ^1H–^{15}N HSQC spectra of *Sc* FAS-holo ACP (black) and *Sc* FAS-holo ACP in the presence of MCAT (red, 1:1.75 molar ratio). Resonances associated with the two phosphopantetheine amines are circled in blue. **b)** Chemical shift changes of the most perturbed residues Asp38, Glu47, Glu52, Lys58, and Ile59. **c)** Weighted chemical shift perturbations of the *Sc* FAS holo ACP in the presence of MCAT. The positions of helices are indicated.

Mapping ACP Residues Involved in MCAT Binding.
The chemical shifts of amide protons are sensitive to changes in environment and conformation and as a result can be used to identify substrate-binding sites. In this work, ^1H–^{15}N HSQC perturbation experiments were used to map the MCAT binding motif on the *Sc* FAS ACP. Ahead of these experiments MCAT activity was confirmed as described previously (data not shown) (5). Uniformly labeled ^{15}N *Sc* FAS holo ACP (initial concentration 250 μM) was titrated with MCAT (stock solution 300 μM) up to an ACP:MCAT ratio of 1:1.75. Overlaying the *Sc* FAS holo ACP spectrum with the titration maximum (Figure 4, panel a) shows that the chemical shift deviations are small for most residues, and only one set of peaks is observed for all residues. This suggests that the structure of bound and unbound ACP is almost identical and that the ACP is in fast exchange between free and bound forms. Small chemical-shift perturbations may also be interpreted as evidence for limited de-

solvation of surface residues (20). These results are consistent with the complex being short-lived. In the presence of MCAT a number of resonances are, however, appreciably perturbed (Figure 4, panel b). The magnitude of these combined chemical shift changes (21) *versus* amino acid sequence position at the titration maximum is shown in Figure 4, panel c. Resonances of the phosphopantetheine chain amide protons undergo no chemical shift change in the presence of MCAT (the cross peaks associated with the two phosphopantetheine amides are indicated with blue circles in Figure 4, panel a), suggesting that the prosthetic group is held away from the enzyme when MCAT lacks malonate.

With the exception of K58 and I59, the most significant chemical shift changes occur in a contiguous region stretching from residue 37, immediately prior to the phosphopantetheine attachment site, continuing up helix II and then across the top of the loop region between helix II and helix III (Figure 4, panel c). Apart from

a 4-residue stretch, immediately prior to helix II, little perturbation of the loop between helices I and II is detected. Our NMR data thus support a model whereby the *Sc* FAS ACP interacts with MCAT through helix II of ACP and encompasses negatively charged residues (Asp40, Glu46, Glu52 and Glu53) that have all been implicated in ACP recognition by ACPS, FabG, and FabH (*1−3*).

Residue Ile54 of *E. coli* ACP showed a significant perturbation on binding to FabG, leading to the suggestion that it might form a hydrophobic contact with the enzyme (*3*). In *Sc* FAS apo ACP, Ile59 (the Ile54 homologue) behaves similarly on binding to MCAT, though this residue is buried and is therefore unable to participate in binding. Homologues of this residue may play a structural role (*22*). This is supported by the observation that the I54A mutant of *Vibrio harveyi* ACP folds incorrectly. It appears likely that the perturbation of Ile59 and Lys58 is due to their location at the hinge between helices II and III, potentially making these residues sensitive to changes in structure and environment. We have recently reported a number of structures for the *Sc* act PKS ACP with bound nonpolar acyl chains and observed large chemical shift changes for the homologous residue Ile60 associated with changes in the φ backbone angle (*23*).

It is significant that the region of the ACP that undergoes the most chemical shift change upon binding to MCAT is that which has the propensity to change conformation (*10, 24*). It is likely, however, that the *Sc* FAS ACP undergoes little change in backbone conformation upon binding and may be limited to side chain rearrangements. Such behavior, although subtle, would be similar to that reported in recent studies of the *Sc* act PKS ACP where side chain rearrangement, particularly of the leucine of the DSL motif, altered the affinity of the protein for ACPS following phosphopantetheinylation (*15*).

Characterization of FAS ACP-MCAT Binding. To determine the role of residues at the interface the conserved residues, *Sc* FAS ACP Asp40, Glu46, Glu52 and Glu53 and MCAT residues Arg189 and Arg287 were mutated. Correct folding was confirmed by circular dichroism (data not shown) as well as $^1H−^{15}N$ HSQC experiments (see Supporting Information). Overall, the mutants appeared to be correctly folded, although the NMR studies did reveal small, localized chemical shift changes arising through alterations in the environment surrounding the mutation. The D40A and E52A FAS ACP mutants showed reduced competence as substrates for

ACPS; D40A FAS ACP was expressed in the inactive apo form, whereas E52A FAS ACP was expressed as a mixture of both apo and holo forms. Complete conversion of E52A FAS ACP was only achieved by incubation of the ACP overnight with a catalytic amount of ACPS and a 5-fold molar excess of Coenzyme A (CoA) (*25*). Under the same conditions the D40A mutant could not be phosphopantetheinylated with *Sc* ACPS, consistent with its location at the ACP-ACPS interface (*1*).

The dissociation constants for the various ACP-MCAT complexes were determined by monitoring the perturbation of the intrinsic tryptophan fluorescence of MCAT upon titration with ACP. We have previously used this technique to study the affinity of ACP for ACPS (*15*). Binding of ACP to MCAT results in the quenching of the intrinsic fluorescence of MCAT (Figure 5, panels a and b). The dissociation constant (K_d, Table 2) was determined as 1.9 ± 0.3 μM. This is consistent with K_d's reported for ACP interaction with other FAS enzymes; for instance, *E. coli* FAS ACP has been reported to bind to FabH with a K_d of 2 ± 1 μM (*2*).

None of the mutations eliminated ACP binding to MCAT entirely. Mutagenesis of Asp40 of the *Sc* FAS ACP DSL motif reduced the affinity of ACP for MCAT (K_d of 13.5 ± 1.4 μM). In part, this reduction may be due to the lack of a phosphopantetheine chain, though from the NMR data presented here we know that the phosphopantetheine chain is held away from MCAT when this enzyme is in its malonate-free form and is unlikely to contribute appreciably to ACP binding. Significantly, Asp40 has been proposed as a point of ACP-MCAT interaction by Keatinge-Clay (*6*), so this mutation alone does not differentiate between this model or one in which helix II of ACP forms the main point of interaction.

Mutagenesis of Arg189 of MCAT (Figure 5, panel b) produces a 5-fold increase in K_d (10 ± 2.7 μM), while the effect of mutating Arg287 is less pronounced (K_d of 3.3 ± 0.5 μM). Mutagenesis of residues Glu46, Glu52, and Glu53 of *Sc* FAS ACP results in a much smaller reduction in the affinity of the ACP for MCAT (Figure 5, panel a, K_d's of 3.0 ± 0.4, 2.7 ± 0.7, and 3.5 ± 0.4 μM, respectively). These results suggest that *Sc* FAS ACP residues Glu46, Glu52, and Glu53 and MCAT residue Arg287 lie at the ACP-MCAT interface but are less significant for high affinity ACP binding than either Asp40 of ACP or Arg189 of MCAT. Reichmann *et al.* have shown that the energetic consequences of deleting residues at a binding site are small if those residues lie within a con-
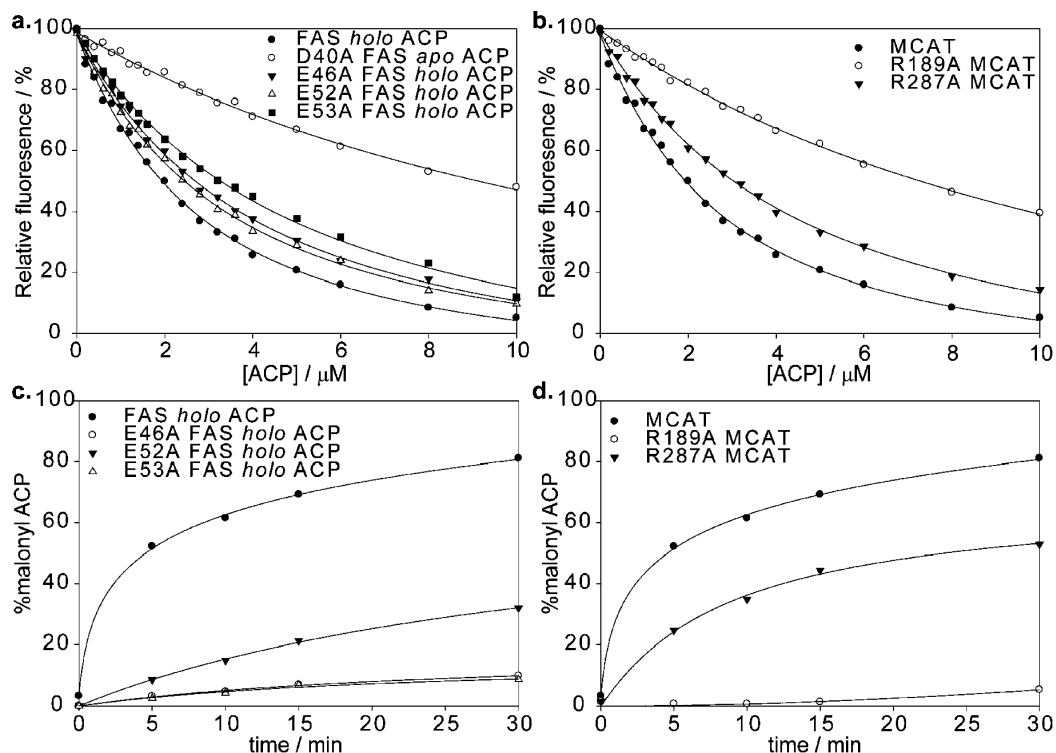
Figure 5. a) Effect of mutagenesis of *Sc* FAS ACP on its ability to bind to MCAT. **b)** Effect of mutagenesis of Arg189 and Arg287 of MCAT on its ability to bind *Sc* FAS holo ACP. In panels a and b fluorescence data is normalized onto a percentage scale based on the maximum (F_{max}) and minimum (F_{min}) fluorescence of the control sample. **c)** Effect of mutagenesis of FAS ACP on its ability to act as a substrate for wild-type MCAT. **d)** Effect of mutagenesis of Arg189 and Arg287 of MCAT on its ability to malonylate *Sc* FAS holo ACP.

tiguous binding site (*26*). Thus, although small, the binding affinity values observed along with the NMR data provide evidence that the FAS ACP interacts through a contiguous binding site.

The ability of the MCAT mutants R189A and R287A to malonylate wild-type *Sc* FAS ACP and of the *Sc* FAS ACP mutants E46A, E52A, and E53A to act as substrates for wild-type and mutated *Sc* MCAT was assayed in a time course assay (Figure 5, panels c and d). In this assay, ACP is incubated with malonyl CoA and a catalytic amount of MCAT, and the formation of malonyl ACP is followed by mass spectrometry (*5*). Under the assay conditions the wild-type MCAT rapidly acylates *Sc* FAS ACP, with almost 70% of the ACP being malonylated within 15 min of the addition of the coenzyme. Malonylation of E46A and E53A *Sc* FAS ACPs is considerably slower than that of the wild-type ACP, with approximately 10% of the ACP acylated over the course of the assay (Figure 5, panel c). Malonylation of E52A *Sc* FAS

ACP is greater than that of E46A and E53A but remains considerably slower than that of the wild-type ACP (approximately 27% of the ACP malonylated, Figure 5, panel c). Mutagenesis of R189 of MCAT resulted in almost complete abolition of its ability to malonylate *Sc* FAS ACP (Figure 5, panel d), whereas R287A acylates approximately half of the *Sc* FAS ACP over the course of the assay. The biological activity of the D40A *Sc* FAS ACP mutant could not be tested as it lacks a phosphopantetheine chain.

Modeling of the MCAT-ACP Complex. On the basis of our mutagenesis and NMR data, a model for the *Sc* FAS ACP-MCAT complex was calculated using the HADDOCK algorithm (*27*). HADDOCK uses NMR data such as chemical shift perturbation or residual dipolar couplings in combination with biochemical data from mutagenesis to define ambiguous distance restraints that describe the role of residues at an interface and has been used to explore the binding of numerous protein

TABLE 2. Dissociation constants for ACP binding to MCAT

ACP	MCAT	K_d (µM)
FAS holo ACP	MCAT	1.9 ± 0.3
D40A FAS apo ACP	MCAT	13.5 ± 1.4
E46A FAS holo ACP	MCAT	3.0 ± 0.4
E52A FAS holo ACP	MCAT	2.7 ± 0.7
E53A FAS holo ACP	MCAT	3.5 ± 0.4
FAS holo ACP	R189A MCAT	10.0 ± 2.7
FAS holo ACP	R287A MCAT	3.3 ± 0.5
C17S act PKS holo ACP	MCAT	3.8 ± 0.6
D41A C17S act PKS apo ACP	MCAT	18.7 ± 2.7
E47A C17S act PKS holo ACP	MCAT	4.7 ± 0.7
E53A C17S act PKS holo ACP	MCAT	4.3 ± 0.3

complexes. Docking was performed using the MCAT crystal structure (PDB code 1nm2) and the closest to average NMR structure of *Sc* FAS apo ACP calculated in this work.

The lowest energy model (Figure 6) suggests that the binding interface between *Sc* FAS ACP and MCAT is in general agreement with one of the initial models provided using Z-DOCK (Figure 3, panel c), though as might be expected, the overall similarity between both models is low (rmsd 7 Å for the superimposition of backbone atoms over the carrier protein structure). The binding interface is small (surface area 669 Å^2) and largely polar in nature. A third of the residues at the interface are hydrophilic, which is consistent with a transient complex (*28*). The *Sc* FAS ACP interacts through salt bridges between helix II on the carrier protein and helix XI and loop 14 of MCAT. Residue Ser41, the ACP phosphopantetheine attachment site, is placed into the active site tunnel of MCAT and locked into position by the formation of a salt bridge between Asp40 of ACP and Lys298 of

MCAT (Figure 6, panel b). This permits the phosphopantetheine chain to extend into the active site tunnel of MCAT, where it can accept malonate, bound at its active site serine (*5*). The importance of this contact is reflected by mutagenesis of Asp40, which significantly affects the ability of MCAT to recognize the *Sc* FAS ACP. Three further salt bridges between Glu46 of ACP and Arg287 of MCAT (Figure 6, panel c), Glu52 of ACP and Lys190 of MCAT, and Glu53 of ACP and Arg189 of MCAT (Figure 6, panel d) serve to hold helix II in place.

One might expect, on the basis of the mutagenesis results described here, that Asp40 of ACP may interact with Arg189 of MCAT. If these residues directly interacted with one another, however, then the phosphopantetheine attachment site would be placed too far from the MCAT active site for malonylation to occur. It seems reasonable to suggest that Arg189 of MCAT can interact with either Glu52 or Glu53 of *Sc* FAS ACP through simple side-chain rearrangement. Mutagenesis of Glu52 or Glu53 individually, therefore, produces a small reduction in affinity as the adjacent residue can replace many of the contacts formed previously by the mutated residue. The principal point of interaction is thus Asp40 of *Sc* FAS ACP with Lys298 of MCAT.

The structure of the malonyl CoA-MCAT complex (*29*) suggests that homologues of Arg189 and Arg287 hold the adenine ring of malonyl CoA in place, guiding the phosphopantetheine portion of CoA to the MCAT active site. This implies a dual role for the arginine residues in both ACP and malonyl CoA binding. Given the Ping Pong Bi Bi mechanism of MCAT this would not be mechanistically problematic as neither malonyl CoA nor CoA are bound at the same time as the *Sc* FAS ACP (*5*). Second, it suggests that our placement of the ACP is correct, as it permits the ACP phosphopantetheine chain to follow the same path as that of malonyl CoA.

Binding of Sc act PKS ACP with MCAT. Analysis of type II PKS gene clusters shows that the majority lack a MCAT homologue, leading a number of groups to propose that *in vivo* the FAS MCAT participates in polyketide biosynthesis (*30*). We therefore investigated the binding affinity of MCAT for the actinorhodin PKS ACP, by tryptophan fluorescence titration (data not shown). The PKS ACP binds to MCAT with approximately half the affinity of the FAS carrier protein with a dissociation constant of 3.8 ± 0.6 µM. It appears that, despite their similarities, structural characteristics of the two ACPs lead to differential binding. Unlike the *Sc* FAS ACP mutagen-
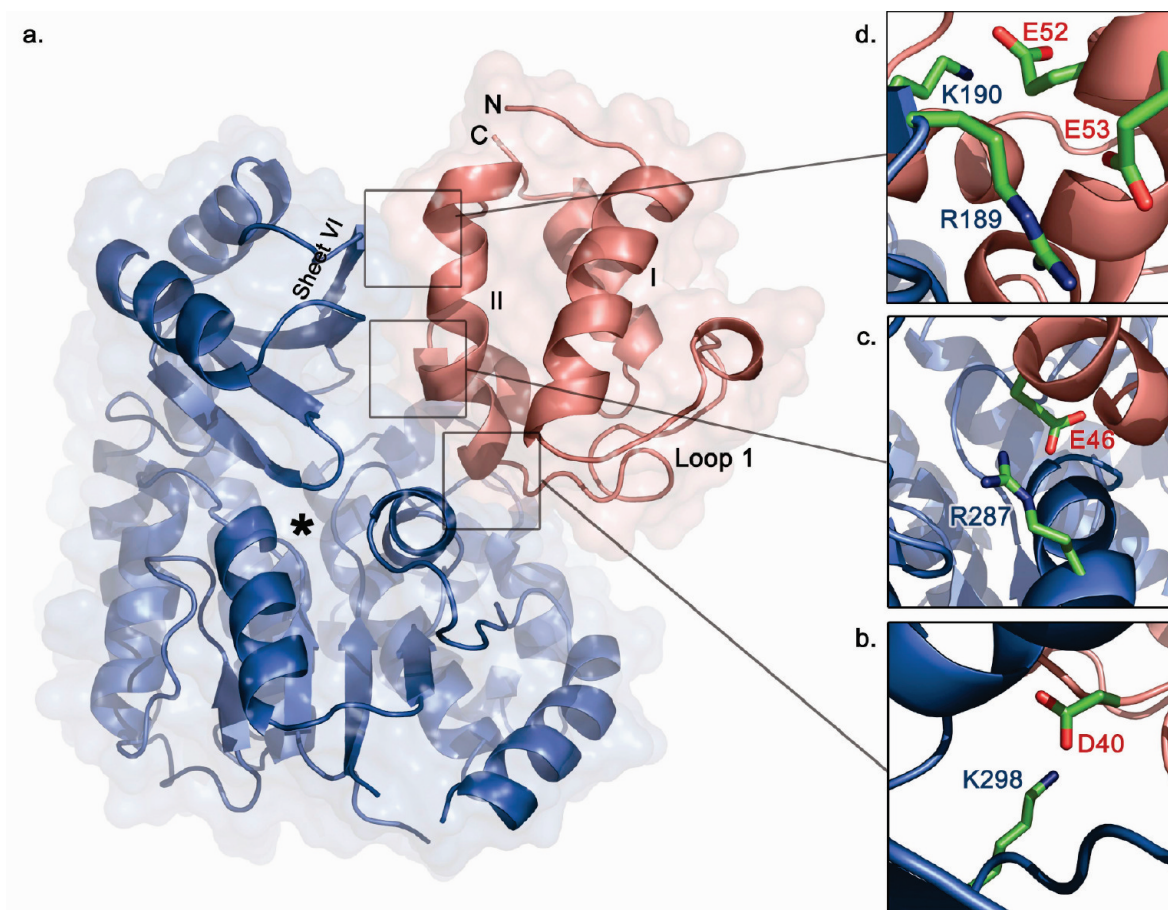
Figure 6. Model of the *Sc* FAS ACP-MCAT complex calculated using HADDOCK (*27*). *Sc* FAS ACP is shown in pink with MCAT in blue. The star indicates the position of the MCAT active site serine. Cutaways show the interaction of negatively charged ACP residues with positively charged residues on MCAT and have been rotated with respect to the main panel to reduce overlap and aid figure clarity.

esis of Glu47 and Glu53 of *Sc* act PKS ACP did little to affect binding to MCAT (dissociation constants of E47A-C17S act PKS ACP and E53A-C17S PKS ACP with MCAT were determined as 4.7 ± 0.7 and 4.3 ± 0.3 μM, respectively, effectively within error of one another and the wild-type act PKS ACP). Mutagenesis of Asp41 of *Sc* act PKS ACP (the *Sc* FAS ACP Asp40 homologue) results in a significant increase in the dissociation constant for the complex (18.7 ± 2.7 μM), suggesting once again that this residue forms the principal contact between ACP and MCAT. Helix II mutations beyond Asp40 therefore have little effect on PKS ACP–MCAT interactions.

The analysis of protein–protein interactions involving FAS ACP clearly points to acidic residues along the length of helix II acting as a universal recognition domain. Positively charged residues around the active sites of interacting enzyme partners can usually be identified, though as yet no common interaction motif has been established (*3*). The results described in this paper confirm these findings for Sc MCAT and Sc FAS ACP and suggest that the ionic interaction with Asp40, the acidic residue adjacent to the active site serine, provides the major point of contact. Evidence for other interactions is limited, though Arg249 of β-ketoacyl-ACP synthase III (FabH) was implicated as the residue critical for the interaction between this enzyme and its cognate carrier protein (*2*). Here *in silico* modeling predicted Glu41 (the Sc FAS ACP Glu46 homologue) as the Arg249 bind-

ing partner, though more extensive ACP interactions could not be ruled out. Finally, mutations of three basic residues at the enoyl reductase (FabI)–ACP helix II interface significantly affected kinetic parameters when compared to the wild-type enzyme (4). Here the Arg204 mutation appeared to be most sensitive to mutation, and analysis of the crystal structure suggested that the binding partner for this residue was Glu48 (the Sc FAS ACP Glu53 homologue). Thus the possibility exists that the principal point of contact may change depending on the ACP-FAS enzyme binding partner.

Conclusion. The recognition of the correct protein partner within a multienzyme complex is vital if the integrity of a biosynthetic sequence is to be maintained and the correct product formed. We have used data gained from NMR experiments, site-directed mutagenesis, and *in vitro* assays to guide the information-driven docking of *Sc* FAS ACP and MCAT and to suggest a biochemically reasonable structure for the complex. This model suggests that the *Sc* FAS ACP recognizes MCAT using a series of conserved glutamic and aspartic acids along helix II that inter-

act with reciprocally charged residues at the mouth of the MCAT active site opening. This mode of binding has also been proposed for ACP recognition by ACPS, FabG, and FabH (1–3).

Except for the mutagenesis of the aspartate of the ACP DSL motif, mutagenesis of helix II residues on the homologous PKS ACP resulted in insignificant changes in MCAT binding affinity. Consequently, the model suggested by Keatinge-Clay *et al.* (6) for the interaction of *Sc* act PKS ACP with MCAT *via* loop I of ACP, or indeed, a binding mode similar to that suggested by the ACP-FabI co-crystal (4), can therefore not be discounted for the binding of this protein to MCAT. It is thus reasonable to suggest that the PKS and FAS ACP may associate with MCAT by different mechanisms, while retaining the principal contact with the aspartate of the ACP DSL motif. The information presented here may provide a useful mechanism for the optimization of specific interactions, allowing, for example, the introduction of alternative acyl transfer enzymes, which may lead to the production of novel compounds.

METHODS

Protein Expression and Purification. All proteins were expressed from *E. coli* strain Bl21(DE3). ACPs were expressed and purified as described previously (25). In this work, the C17S mutant of act PKS ACP has been used throughout in order to prevent intramolecular disulfide bond formation between Cys17 and the thiol of the phosphopantetheine chain (31). This mutant behaves in all regards like the wild-type ACP. Single ^{15}N- or double ^{15}N/^{13}C-labeled *Sc* FAS holo ACP was expressed in M9 minimal media with ^{15}N ammonium chloride and ^{13}C glucose as the sole nitrogen and carbon source, respectively. *Sc* MCAT enzymes were expressed in a hexa-histidine-tagged form and purified by nickel affinity chromatography as described previously (5). The hexa-histidine tag was not removed prior to biochemical studies.

Mutagenesis and Sequencing. Mutants were prepared using the Stratagene Quikchange method as outlined in the manufacturer's protocol. Complementary oligonucleotide primers of the following sequences were synthesized by Sigma Genosys: D40A FAS FOR 5′-CGACGTC GCT TCGCTGTCC-3′, D40A FAS REV, CGA-CAGCGA AGC GACGTCC-3′; E46A FAS FOR 5′-CGCTGTCCATGGTC GCT GTCGTCGTCGC-3′, E46A FAS REV 5′-GCGACGACGAC AGC GACCATGGACAGCG-3′; E52A FAS FOR 5′-GTCGCCGCCGCC GCT GAGCGCTTC, E52A FAS REV 5′-GAAGCGCTC AGC GGCGGCGGC-GAC-3′; R189A MCAT FOR 5′-GCCCGAGGGTGTG GCT AAGG-TCGTCCCGCTG-3′, R189A MCAT REV 5′-CAGCGGGACGACCTT AGC CACACCCTCGGGC-3′; R287A MCAT FOR 5′-GGGCTGGCCAAG GCT GCGCTGCCCGGAGTG-3′, R287A MCAT REV 5′-CACTCCGGGCA-GCGC AGC CTTGGCCAGCCC-3′. The resultant plasmids were sequenced (Cogenics, U.K.) to confirm mutagenesis.

NMR of Sc FAS-ACP. For *Sc* FAS ACP structural studies, standard triple resonance experiments were acquired for sequential and side-chain assignment on a Varian INOVA 600 MHz spectrometer. Structural restraints were acquired from a single ^{13}C/

^{15}N NOESY-HSQC (32). For the noncovalent binding studies, standard sensitivity enhanced HSQC spectra were acquired. Spectra were processed and viewed with nmrPipe (33), Sparky (34), and Analysis (35). All structure calculations were carried out using the ARIA protocol Version 1.2 (9).

Mass Spectrometry. Electrospray mass spectrometry (ESMS) was used for the analysis of protein samples after purification or in our standard discontinuous assays. For ESMS analysis all samples were desalted and concentrated on C4 chromatographic resin. Proteins were ionized with a Nanomate chip based nanoflow source, using a pressure of 0.3 psi and a spray voltage of between 1.4 and 1.6 kV, and analyzed in positive ion mode on a Applied Biosystems QStar XL mass spectrometer.

Sc MCAT Catalyzed Malonylation of ACP. Purified MCAT was assayed for its ability to malonylate FAS ACP. Briefly, FAS holo ACP was treated with dithiothreitol to reduce any disulfide bonds, and this reduced ACP (50 μM) was incubated with malonyl CoA (50 μM) and MCAT (0.1 nM) at 30 °C in potassium phosphate buffer (100 mM, pH 7.3) and glycerol (10% v/v). Reactions were quenched at 0, 5, 15, and 30 min and prepared for ESMS.

Tryptophan Fluorescence Titration. All fluorescence spectra were recorded using a Spex Fluoromax spectrophotometer (Jobin Yvon). Tryptophan fluorescence was excited at 295 nm and measured over 280–420 nm, using a slit width of 0.75 μm, integrating over 1 s. *Sc* MCAT (1 μM, 2 mL) was titrated with monomerised holo ACP (200 μM stock) to a total ACP concentration of 10 μM. All assays were performed at 25 °C in potassium phosphate buffer (100 mM, pH 7.3) containing glycerol (10% v/v) and dithiothreitol (1 mM).

Macromolecular Docking of FAS ACP and MCAT. Docking was performed using both the MCAT crystal structure and the closest to average NMR structure of *Sc* FAS apo ACP calculated in this work. The proteins were docked with one another using ZDock (16), GRAMM-X (17), and ClusPro (18) following the stan-

dard protocols for each package. For the information-driven docking of ACP and MCAT the protein–protein docking program HADDOCK was used (27). Crystallographic waters and metal ions were removed from the MCAT PDB file prior to docking. Mutagenesis and chemical shift perturbation data for residues at the interface were used to define a series of ambiguous interaction restraints. Active residues were defined as those having chemical shift perturbations larger than the average and a relative residue accessible surface area larger than 50%. Surface accessible residues adjacent to the active residues were defined as passive. During docking calculations helix II of ACP and the regions surrounding Arg189 and Arg287 on MCAT were considered flexible. One thousand rigid-body solutions were generated. The best 200 were refined in torsion angle space and in water.

Supporting Information Available: This material is available free of charge *via* the Internet at http://pubs.acs.org.

REFERENCES

1. Parris, K. D., Lin, L., Tam, A., Mathew, R., Hixon, J., Stahl, M., Fritz, C. C., Seehra, J., and Somers, W. S. (2000) Crystal structures of substrate binding to *Bacillus subtilis* holo-(acyl carrier protein) synthase reveal a novel trimeric arrangement of molecules resulting in three active sites, *Structure 8*, 883–895.

2. Zhang, Y. M., Rao, M. S., Heath, R. J., Price, A. C., Olson, A. J., Rock, C. O., and White, S. W. (2001) Identification and analysis of the acyl carrier protein (ACP) docking site on β-ketoacyl-ACP synthase III, *J. Biol. Chem. 276*, 8231–8238.

3. Zhang, Y. M., Wu, B., Zheng, J., and Rock, C. O. (2003) Key residues responsible for acyl carrier protein and β-ketoacyl-acyl carrier protein reductase (FabG) interaction, *J. Biol. Chem. 278*, 52935–52943.

4. Rafi, S., Novichenok, P., Kolappan, S., Zhang, X., Stratton, C. F., Rawat, R., Kisker, C., Simmerling, C., and Tonge, P. J. (2006) Structure of acyl carrier protein bound to FabI, the FASII enoyl reductase from *Escherichia coli*, *J. Biol. Chem. 281*, 39285–39293.

5. Szafranska, A. E., Hitchman, T. S., Cox, R. J., Crosby, J., and Simpson, T. J. (2002) Kinetic and mechanistic analysis of the malonyl CoA:ACP transacylase from *Streptomyces coelicolor* indicates a single catalytically competent serine nucleophile at the active site, *Biochemistry 41*, 1421–1427.

6. Keatinge-Clay, A. T., Shelat, A. A., Savage, D. F., Tsai, S. C., Miercke, L. J., O'Connell, J. D., 3rd, Khosla, C., and Stroud, R. M. (2003) Catalysis, specificity, and ACP docking site of *Streptomyces coelicolor* malonyl-CoA:ACP transacylase, *Structure 11*, 147–154.

7. Zhang, L., Liu, W., Xiao, J., Hu, T., Chen, J., Chen, K., Jiang, H., and Shen, X. (2007) Malonyl-CoA:acyl carrier protein transacylase from *Helicobacter pylori*: crystal structure and its interaction with acyl carrier protein, *Protein Sci. 16*, 1184–1192.

8. Arthur, C. J., Szafranska, A., Evans, S. E., Findlow, S. C., Burston, S. G., Owen, P., Clark-Lewis, I., Simpson, T. J., Crosby, J., and Crump, M. P. (2005) Self-malonylation is an intrinsic property of a chemically synthesized type II polyketide synthase acyl carrier protein, *Biochemistry 44*, 15414–15421.

9. Rieping, W., Habeck, M., Bardiaux, B., Bernard, A., Malliavin, T. E., and Nilges, M. (2007) ARIA2: automated NOE assignment and data integration in NMR structure calculation, *Bioinformatics 23*, 381–382.

10. Zornetzer, G. A., Fox, B. G., and Markley, J. L. (2006) Solution structures of spinach acyl carrier protein with decanoate and stearate, *Biochemistry 45*, 5217–5227.

11. Koglin, A., Mofid, M. R., Löhr, F., Schafer, B., Rogov, V. V., Blum, M. M., Mittag, T., Marahiel, M. A., Bernhard, F., and Dotsch, V. (2006) Conformational switches modulate protein interactions in peptide antibiotic synthetases, *Science 312*, 273–276.

12. Xu, G. Y., Tam, A., Lin, L., Hixon, J., Fritz, C. C., and Powers, R. (2001) Solution structure of *B. subtilis* acyl carrier protein, *Structure 9*, 277–287.

13. Qiu, X. Y., and Janson, C. A. (2004) Structure of apo acyl carrier protein and a proposal to engineer protein crystallization through metal ions, *Acta Crystallogr., Sect. D: Biol. Crystallogr. 60*, 1545–1554.

14. Crump, M. P., Crosby, J., Dempsey, C. E., Parkinson, J. A., Murray, M., Hopwood, D. A., and Simpson, T. J. (1997) Solution structure of the actinorhodin polyketide synthase acyl carrier protein from *Streptomyces coelicolor* A3(2), *Biochemistry 36*, 6000–6008.

15. Evans, S. E., Williams, C., Arthur, C. J., Burston, S. G., Simpson, T. J., Crosby, J., and Crump, M. P. (2008) An ACP structural switch: conformational differences between the Apo and Holo forms of the actinorhodin polyketide synthase acyl carrier protein, *ChemBioChem 9*, 2424–2432.

16. Chen, R., Li, L., and Weng, Z. (2003) ZDOCK: an initial-stage protein-docking algorithm, *Proteins 52*, 80–87.

17. Tovchigrechko, A., and Vakser, I. A. (2006) GRAMM-X public web server for protein-protein docking, *Nucleic Acids Res. 34*, W310–314.

18. Comeau, S. R., Gatchell, D. W., Vajda, S., and Camacho, C. J. (2004) ClusPro: an automated docking and discrimination method for the prediction of protein complexes, *Bioinformatics 20*, 45–50.

19. Janin, J., Henrick, K., Moult, J., Eyck, L. T., Sternberg, M. J., Vajda, S., Vakser, I., and Wodak, S. J. (2003) CAPRI: a Critical Assessment of PRedicted Interactions, *Proteins 52*, 2–9.

20. Crowley, P. B., and Ubbink, M. (2003) Close encounters of the transient kind: protein interactions in the photosynthetic redox chain investigated by NMR spectroscopy, *Acc. Chem. Res. 36*, 723–730.

21. Pellecchia, M., Sebbel, P., Hermanns, U., Wüthrich, K., and Glockshuber, R. (1999) Pilus chaperone FimC-adhesin FimH interactions mapped by TROSY-NMR, *Nat. Struct. Biol. 6*, 336–339.

22. Flaman, A. S., Chen, J. M., Van Iderstine, S. C., and Byers, D. M. (2001) Site-directed mutagenesis of acyl carrier protein (ACP) reveals amino acid residues involved in ACP structure and acyl-ACP synthetase activity, *J. Biol. Chem. 276*, 35934–35939.

23. Evans, S. E., Williams, C., Arthur, C. J., Ploskon, E., Wattana-amorn, P., Cox, R. J., Crosby, J., Willis, C. L., Simpson, T. J., and Crump, M. P. (2009) Probing the interactions of early polyketide intermediates with the actinorhodin ACP from *S. coelicolor* A3(2), *J. Mol. Biol. 389*, 511–528.

24. Roujeinikova, A., Simon, W. J., Gilroy, J., Rice, D. W., Rafferty, J. B., and Slabas, A. R. (2007) Structural studies of fatty acyl-(acyl carrier protein) thioesters reveal a hydrophobic binding cavity that can expand to fit longer substrates, *J. Mol. Biol. 365*, 135–145.

25. Cox, R. J., Crosby, J., Daltrop, O., Glod, F., Jarzabek, M. E., Nicholson, T. P., Reed, M., Simpson, T. J., Smith, L. H., Soulas, F., Szafranska, A. E., and Westcott, J. (2002) *Streptomyces coelicolor* phosphopantetheinyl transferase: a promiscuous activator of polyketide and fatty acid synthase acyl carrier proteins, *J. Chem. Soc., Perkin Trans. 1* 1644–1649.

26. Reichmann, D., Rahat, O., Albeck, S., Meged, R., Dym, O., and Schreiber, G. (2005) The modular architecture of protein-protein binding interfaces, *Proc. Natl. Acad. Sci. U.S.A. 102*, 57–62.

27. Dominguez, C., Boelens, R., and Bonvin, A. M. (2003) HADDOCK: a protein-protein docking approach based on biochemical or biophysical information, *J. Am. Chem. Soc. 125*, 1731–1737.

28. Keskin, O., and Nussinov, R. (2007) Similar binding sites and different partners: implications to shared proteins in cellular pathways, *Structure 15*, 341–354.

29. Oefner, C., Schulz, H., D'Arcy, A., and Dale, G. E. (2006) Mapping the active site of *Escherichia coli* malonyl-CoA-acyl carrier protein transacylase (FabD) by protein crystallography, *Acta Crystallogr., Sect. D: Biol Crystallogr. 62*, 613–618.

30. Revill, W. P., Bibb, M. J., and Hopwood, D. A. (1995) Purification of a malonyltransferase from *Streptomyces coelicolor* A3(2) and analysis of its genetic determinant, *J. Bacteriol. 177*, 3946–3952.

31. Hitchman, T. S., Crosby, J., Byrom, K. J., Cox, R. J., and Simpson, T. J. (1998) Catalytic self-acylation of type II polyketide synthase acyl carrier proteins, *Chem. Biol. 5*, 35–47.

32. Pascal, S. M., Muhandiram, D. R., Yamazaki, T., Forman-Kay, J. D., and Kay, L. E. (1994) Simultaneous acquisition of N-15-edited and C-13-edited NOE spectra of proteins dissolved in H_2O, *J. Magn. Reson., Ser. B 103*, 197–201.

33. Delaglio, F., Grzesiek, S., Vuister, G. W., Zhu, G., Pfeifer, J., and Bax, A. (1995) NMRPipe: a multidimensional spectral processing system based on UNIX pipes, *J. Biomol. NMR 6*, 277–293.

34. Goddard, T. D., Kneller, D. G. *Sparky 3*, University of California, San Francisco, CA.

35. Vranken, W. F., Boucher, W., Stevens, T. J., Fogh, R. H., Pajon, A., Llinas, M., Ulrich, E. L., Markley, J. L., Ionides, J., and Laue, E. D. (2005) The CCPN data model for NMR spectroscopy: development of a software pipeline, *Proteins 59*, 687–696.

36. DeLano, W. L. (2002) *The PyMOL Molecular Graphics System*, DeLano Scientific, San Carlos, CA.